Talanta 107 (2013) 195–202

Contents lists available at SciVerse ScienceDirect

Talanta

journal homepage: www.elsevier.com/locate/talanta

Direct electron transfer of cytochrome *c* at mono-dispersed and negatively charged perylene–graphene matrix

Nan Zhang [a], Xiangyu Lv [a], Weiguang Ma [a], Yuwei Hu [a], Fenghua Li [a], Dongxue Han [a,*], Li Niu [a,b]

[a] State Key Laboratory of Electroanalytical Chemistry, c/o Engineering Laboratory for Modern Analytical Techniques, Changchun Institute of Applied Chemistry, Chinese Academy of Sciences, Changchun 130022, PR China

[b] Changzhou Institute of Energy Storage Materials and Devices, Changzhou 213001, PR China

ARTICLE INFO

Article history:
Received 10 September 2012
Received in revised form
18 December 2012
Accepted 21 December 2012
Available online 29 December 2012

Keywords:
Cytochrome *c*
Direct electron transfer
3,4,9,10-perylene tetracarboxylic acid
Graphene

ABSTRACT

Mono-dispersed 3,4,9,10-perylene tetracarboxylic acid (PTCA) functionalized graphene sheets (PTCA-graphene) were fabricated by a chemical route and dispersed well in aqueous solution. PTCA-graphene with plenty of –COOH groups as electrostatic absorbing sites were beneficial to the loading of Cytochrome c (Cyt *c*). Cyt *c*, which was tightly immobilized on the PTCA-graphene modified glassy carbon electrode, maintained its natural conformation. Direct electron transfer of Cyt *c* and the electrocatalytic activity towards the reduction of H_2O_2 were also achieved. It has been substantiated that PTCA-graphene is a preferable biocompatible matrix for Cyt *c*.

1. Introduction

Cytochrome *c* (Cyt *c*), whose function is to receive electrons from Cyt *c* reductase and deliver them to Cyt *c* oxidase, plays an important role in the respiration chain. Just like other heme-containing proteins, such as myoglobin and horseradish peroxidase, Cyt *c* has the ability to electro-catalyze the reduction of hydrogen peroxide (H_2O_2) [1]. It has been previously reported to detect some other small molecules including nitrite salt [2], nitric oxide [3], superoxide radical anion [4] etc. Furthermore, Cyt *c* can be a powerful tool to make sensitive electrochemical biosensor devices [5]. To realize this application, electrochemical research on the electron transfer of Cyt *c* at electrode/solution interfaces is indispensable. However, Proteins are huge molecules and the electro-active centers are usually embedded deeply into the large three dimensional structures of enzyme molecules [6]. It is difficult for electrons to transfer from the redox center of protein to the surface of the electrode. To efficiently achieve the direct electron transfer (DET) of Cyt *c* and realize its potential applications for electrochemical biosensors, different kinds of nanomaterials have been employed as media or matrix, such as gold nanoparticles (GNPs) [7,8], cobalt oxide nanoparticles [9], silicon nanotubes [10], single-walled carbon nanotubes (SWNT) [11,12], and multi-walled carbon nanotubes (MWNT) [13], etc. In fact, it has been investigated and concluded that these nanomaterials acted as "tiny conducting wires" leading between the protein center and the electrode.

Meanwhile, how to immobilize Cyt *c* to the electrode is another key challenge to its application for electrochemical biosensors. The importance of binding between protein and electrode as a prerequisite for electron transfer has been previously discussed [14]. In order to conquer the unfavorable orientation of Cyt *c* at the surface of the electrode and maintain its natural activity, researchers have tried to find several effective approaches to immobilize Cyt *c* onto the surface of the electrode [15–18]. The electrostatic interaction between Cyt *c* and electrode surface plays a key role during the redox reaction of Cyt *c* [19–22]. Cyt *c* with a high PI (>10) is positively charged in neutral conditions. Chen and coworkers mixed negatively charged DNA with carbon nanotubes to perform a preferable matrix which could strongly adsorb Cyt *c* [21]. Armstrong found that the electron transfer rate of Cyt *c* on the edge which has higher surface O/C ratio was 2-folds higher than that on the basal plane of pyrolytic graphite [19]. Kasmi and coworkers have investigated the changes of the electron transfer rates when $-COO^-$ terminated self-assembled monolayer surface mixed with hydroxyl groups [16]. According to these reports, introducing negatively charged –COOH groups to the substrate might be an effective way to promote the loading of Cyt *c* and facilitate the redox reaction of Cyt *c*.

Among different kinds of nanomaterials, graphene is an ideal candidate to achieve the functions as "conducting wire" and serve as good substrate simultaneously. Graphene has the unique structure of single layer of carbon atoms in a closely packed

* Corresponding author. Fax: +86 431 8526 2800.
E-mail address: dxhan@ciac.jl.cn (D. Han).

0039-9140/$ - see front matter © 2012 Elsevier B.V. All rights reserved.
http://dx.doi.org/10.1016/j.talanta.2012.12.028

honeycomb two-dimensional lattice. This structure helps graphene expose itself completely to the analyte and provide more active sites essential for the redox reaction. According to the literature, graphene has a higher surface area which can afford a higher loading capacity for enzyme comparing with carbon nanotubes [23]. Meanwhile, its excellent conductivity can facilitate the electrons transfer from the biomolecules [24]. And its biocompatibility was demonstrated by Chen and coworkers based on the cell culture experiments [25]. These exceptional properties of graphene provide it potential applicability in the applications in electrochemical biosensors. Till now, researchers have developed the graphene-based glucose biosensor [26,27], H_2O_2 biosensor [28,29], NADH biosensor [30], Cholesterol biosensor [31] etc. However, the advantages of graphene are only associated with individual sheets. Due to the high cohesive van der Waals energy and strong π–π stacking, graphene sheets will agglomerate irreversibly without any protections. Therefore, in order to obtain graphene materials with good dispersibilities as well as excellent properties, covalent modifications [32,33] or noncovalent functionalizations [24,34,35] of graphene have been performed.

In this work, –COOH groups have been introduced to graphene sheets by functionalization with 3,4,9,10-perylene tetracarboxylic acid (PTCA) which contains a π-conjugated perylene ring and four carboxyl groups. The composite has plenty of electrostatic interaction sites for the loading of Cyt *c*. Meanwhile it has the superb dispersibility which can provide high conductivity and high surface area. During the electrochemical investigations, a pair of well-defined and symmetric redox peaks corresponding to the oxidation and reduction of the iron in the heme group of Cyt *c* was obtained at the PTCA-graphene modified glassy carbon electrode (GCE). Cyt *c* on the modified electrode showed its native properties. It electrochemically catalyzed the reduction of H_2O_2. PTCA-graphene was proved to be a preferable substrate and "conducting wire" simultaneously. It played an important role in the DET between active center of Cyt *c* and electrode surface. The monodispersibility and negative charge make this material a suitable candidate for the substrate of other biosensors.

2. Materials and methods

2.1. Chemicals

Horse heart Cyt *c* (96%, Mw 12,384) and 3,4,9,10-perylenetetracarboxylic dianhydride (PTCDA,97%) were obtained from Sigma. Graphite powders (spectral requirement) were purchased from Shanghai chemicals, China. Hydrazine solution (50 wt%) was purchased from Beijing Yili Chemicals, China. Ammonia solution (28 wt%) and hydrogen peroxide solution (30 wt%) were obtained from Beijing Chemicals, and a fresh solution of H_2O_2 was prepared daily. Phosphate buffer solutions (PBS, 20 mM) with various pH values were prepared by mixing stock standard solutions of Na_2HPO_4 and NaH_2PO_4. Acetic acid-sodium acetate buffer solution was prepared with stock standard solutions of HAc and NaAc. Unless otherwise stated, reagents were of analytical grade and used as received. All aqueous solutions were prepared with doubly distilled water from a Millipore system (>18 MΩ/cm).

2.2. Apparatus

UV–vis absorption spectra were recorded using a Cary 500 UV/vis/near-IR spectrometer. Fourier transform infrared spectroscopy (FTIR) was performed on a Bruker Vertex 70 spectrometer. Scanning electron microscopy (SEM) pictures were imaged by a field emission scanning electron microscopy (FE-SEM, XL30ESEM-FEG). AFM images were obtained with a Digital Instruments nanoscope IIIa (Multimode, Veeco), operating in tapping mode.

Cyclic voltammetry (CV) measurements were performed with CHI 660A electrochemical workstation (CHI, USA). Electrochemical impedance spectroscopy (EIS) measurements were carried out with Solartron 1255B Frequency Response Analyzer (Solartron Inc., UK). All the electrochemical experiments were performed using a conventional three electrode cell with bare or modified GCE ($d=3$ mm) as the working electrode, a Pt coil as the counter electrode and Ag/AgCl (3 M KCl) as the reference electrode. Before use, the GCE was mechanically polished with alumina slurries (1, 0.3, 0.05 μm) to a mirror successfully, and sonicated in ultrapure water for several times.

2.3. Electrochemical measurements

Unless otherwise stated, the electrolyte solution used for all electrochemical experiments was a 0.02 M, pH 7.4 PBS. EIS measurements were performed in the presence of 5 mM $K_3[Fe(CN)_6]$/$K_4[Fe(CN)_6]$ (1:1) and 0.1 M KCl by applying an alternating current (AC) voltage with 5 mV amplitude in a frequency range from 0.1 Hz to 10 kHz under open circuit potential conditions. Prior to electrochemical experiments, all the solutions were deaerated with high purity nitrogen and maintained under nitrogen atmosphere during measurements. All the electrochemical experiments were carried out at room temperature.

2.4. PTCA-graphene fabrication

Functionalization of graphene with PTCA was conducted according to our previous work [36,37]. First, graphene oxides (GO) were synthesized from natural graphite powder by a modified Hummers method which was originally presented by Kovtyukhova and colleagues [38]. The PTCA solution was made by hydrolyzing PTCDA in a minimal volume of 1.0 M sodium hydroxide [39]. Red depositions appeared in the yellow–green solution and were collected by centrifugation and dried under vacuum at room temperature. 21.2 mg graphene oxide and 5.2 mg PTCA were dissolved in 20.0 mL water by ultrasonication, and then stirred at 40 °C overnight. Subsequently, 26.8 μL hydrazine solution and 0.30 mL ammonia solution were added to the above solution and the resulting mixture was held at 95 °C for 30 min under vigorous agitation. The product was subsequently filtered by a Nylon membrane with *ca.* 0.22 μm pores and thoroughly washed with ultrapure water and dried under vacuum at room temperature. As controlled experiment, pristine graphene was obtained by the similar procedure without addition of PTCA to the blank sample.

2.5. Preparation of modified electrode

Cyt *c* solution (10 mg/mL in PBS, 20 mM, pH 7.4) and PTCA-graphene suspension (0.4 mg/mL) were mixed by the volume ratio of 2:3 at the room temperature with constant stirring for 5 min. Then 5 μL of the mixed solution was drop-cast on the surface of the electrodes which were allowed to be dried at room temperature.

3. Result and discussion

3.1. Characterizations of PTCA functionalized graphene

The preparation of PTCA-graphene is illustrated in Scheme 1. The PTCA molecules carried –COOH groups and interacted with the basal plane of graphene sheets by π–π stacking and hydrophobic

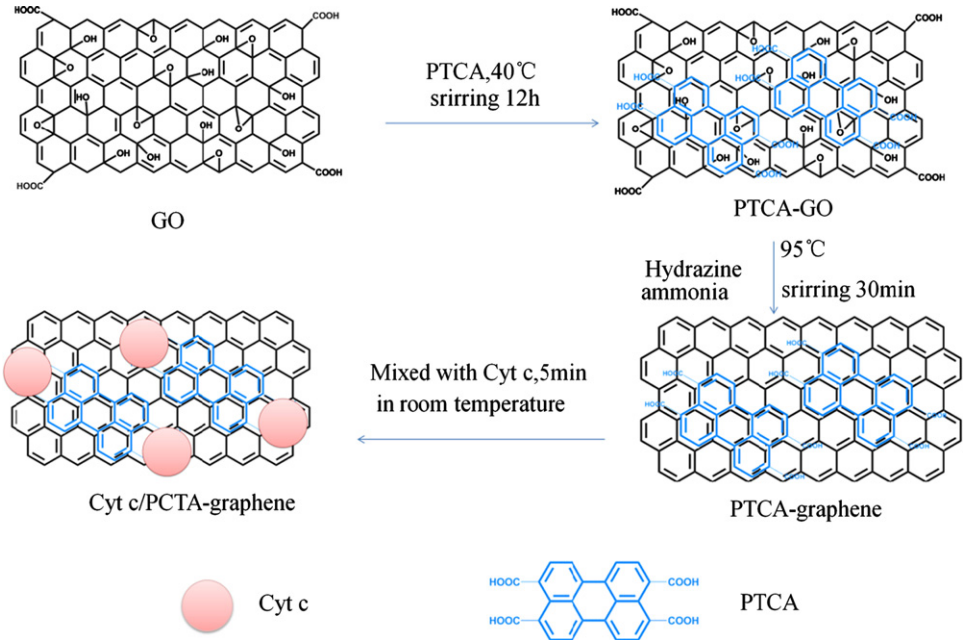

Scheme 1. Schematic representation of PTCA-graphene's preparation and its immobilization with Cyt *c*.

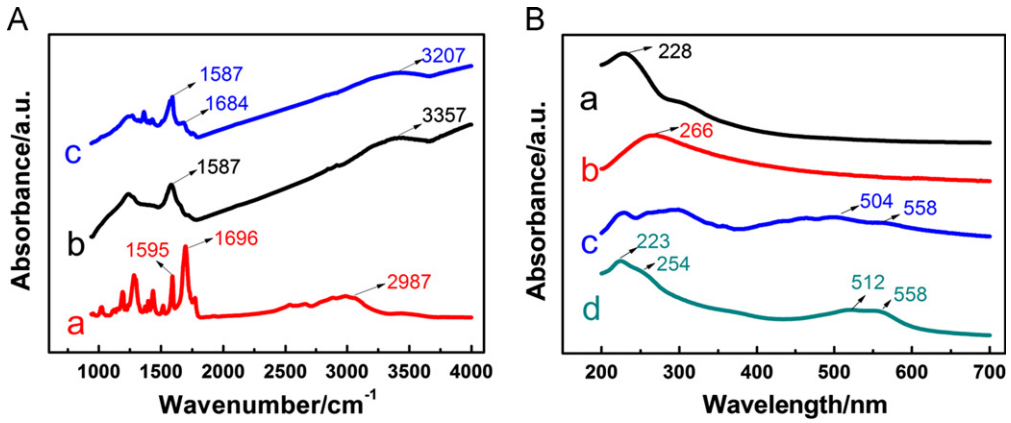

Fig. 1. (A) FTIR spectra of PTCA (a), graphene (b), and PTCA-graphene (c). (B) UV–vis absorption spectra of GO (a), graphene (b), PTCA (c) and PTCA-graphene (d).

forces [36]. As shown, through π–π stacking and hydrophobic effect, the conjugated rings of PTCA could interact with the basal plane of graphene sheets. PTCA-graphene sheets played a key role in the DET between the active center of Cyt *c* and electrode surface.

FTIR and UV–vis were performed to further confirm the formation of PTCA-graphene. As is shown in the FTIR spectra (Fig. 1A), ν(C=C) stretching vibration peaks usually appear in a wavenumber region of 1680–1600 cm^{-1}. The wavenumber is lower when the conjugation degree is higher. At this point, 1595 cm^{-1} (a) was ascribed to the aromatic ν(C=C) stretching vibration of PTCA [40] and 1587 cm^{-1} (b and c) was corresponding to the ν(C=C) stretching vibration of graphene with a π-conjugation network. Since ν(C=O) peaks usually appear in a wavenumber region of 1680–1700 cm^{-1}, the peak 1696 cm^{-1} (a) was assigned to ν(C=O) vibration of PTCA. The characteristic peaks of PTCA (1684 cm^{-1}) observed in the spectra of PTCA-graphene (c) suggested the presence of –COOH groups on the PTCA-graphene sheets and the successful conjugation of PTCA and graphene. The ν(C=O) peaks of PTCA-graphene shifted to 1684 cm^{-1} (c), which might be attributed to the π–π stacking and hydrophobic forces between PTCA and graphene.

The UV–vis absorption spectra of GO, graphene, PTCA and PTCA-graphene were characterized and shown in Fig. 1B. The strong absorption band at 228 nm (a) attributing to π–π^* transitions of aromatic C=C bonds. The aromatic C=C bonds of graphene red shifted to 266 nm (b) after reduction elucidating the reversion of a π-conjugation network. The spectrum of PTCA-graphene contained a strong band at 223 nm, a weak band around 254 nm (d), and the characteristic peaks of PTCA (512 and 558 nm c), which were similar to the previous report [37], indicating the binding of PTCA with graphene.

Despite the evidences from FTIR and UV–vis spectra which have confirmed the successfully functionalization of graphene by PTCA, there were also some visualized proofs. Since the –COOH groups of PTCA can afford PTCA-graphene sheets negative charges and caused electrostatic repulsion between the individual sheets. The functionalized composite demonstrated a better dispersibility and stability than the pristine graphene, which was substantiated by the digital photographs (shown in Fig. 2A). Compared to the solution of pristine graphene (b), solution of PTCA-graphene (a) with –COOH groups was found still pellucid and well dispersed after 39 days. SEM images of PTCA-graphene and graphene were showed in Fig. 2B. Graphene film (b) looked like a wrinkling

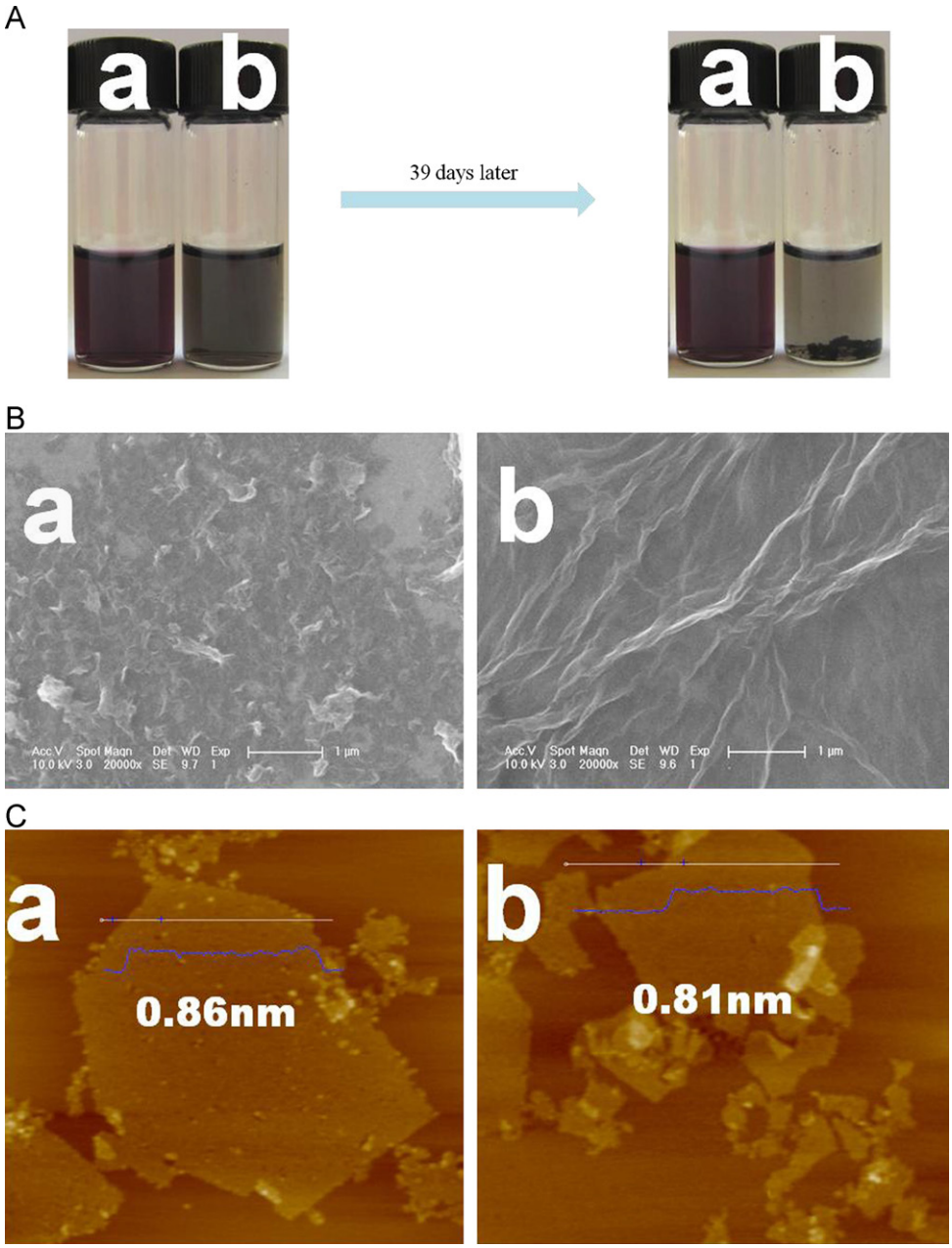

Fig. 2. (A) Digital photographs of PTCA-graphene (a) and graphene (b). (B) SEM images of PTCA-graphene (a) and graphene (b). (C) Tapping-mode AFM image of PTCA-graphene (a) and graphene (b).

paper. PTCA-graphene film (a) showed a flake-like shape which was significantly different from that of graphene. AFM images of the PTCA-graphene (a) and pristine graphene (b) sheets were shown in Fig. 2C. The thickness of PTCA-graphene film was 0.86 nm while pristine graphene film was 0.81 nm. This indicated that they were both single layers as previously reported [41,42]. The increase of the height indicated the attachment of PTCA to graphene.

3.2. Spectroscopic analysis of the association of the Cyt c and PTCA-graphene

Since maintaining the native three-dimensional structures of proteins is the prerequisite of their applications, the biocompatibility of PTCA-graphene is of great importance. According to literatures, Soret band (408 nm) and the weak Q band (529 nm) produced by the chromophore of porphyrin [43] are the characteristic bands of native Cyt *c*. The position of them can provide information about possible denaturation of conformational change in the heme group region [44]. Correspondingly, 409 and 527 nm showed in the spectra of Cyt *c* in our characterizations (Fig. 3a) were ascribed to the Soret band and Q band, respectively. While after mixing with PTCA-graphene (Fig. 3b), these two characteristics bands were unaltered, which suggested that Cyt *c* can maintain its native state after interacted with PTCA-graphene. The above comparison further illustrated the biocompatibility of PTCA-graphene as well.

3.3. Electrochemical impedance characterization of Cyt c/PTCA-graphene/GCE

The immobilization of Cyt *c* to the electrode was investigated by EIS. EIS is an effective approach to probe the change on the surface of the electrode. Graphene, PTCA-graphene and Cyt *c*/PTCA-graphene modified GCE were examined by exploiting the

solution-based redox probe $[Fe(CN)_6]^{3-/4-}$ (Fig. 4). In the EIS, the semicircle part at high frequencies corresponds to the electron transfer limiting process. And the electron transfer resistant (R_{ct}) can be directly measured as the semicircle diameter. When PTCA-graphene was modified onto the GCE surface (c), the R_{ct} value increased obviously as compared to the graphene modified GCE (b). This suggested the successful functionalization of graphene sheets, since the plenty of negatively charged –COOH prevented $[Fe(CN)_6]^{3-/4-}$ from reaching the electrode [13,45]. After coated with Cyt *c*/PTCA-graphene film (d), the inter-facial resistance increased resulting from the hindered pathway of electron transfer by Cyt *c* which embodied the insulating property of proteins. These results attested that the Cyt *c* was successfully immobilized on the modified GCE.

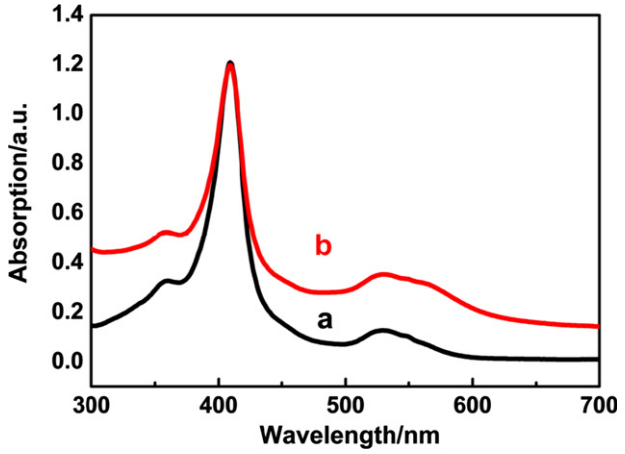

Fig. 3. The UV–vis absorption spectra of Cyt *c* in PBS (20 mM, pH 7.4) without (a) and with PTCA-graphene (b).

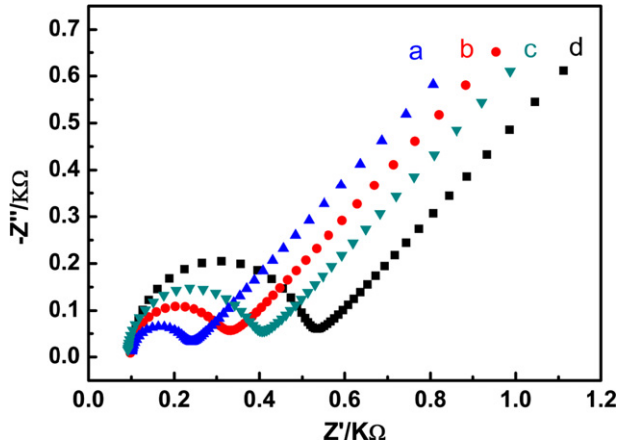

Fig. 4. The Nyquist diagram of the modified GCE in the presence of 5.0 mM $[Fe(CN)_6]^{3-/4-}$ (1:1) solution containing 0.1 M KCl. Bare GCE (a), graphene/GCE (b), PTCA-graphene/GCE (c) and Cyt *c*/PTCA-graphene/GCE (d).

3.4. DET of Cyt c on the Cyt c/PTCA-graphene/GCE

The electrochemistry behaviors of Cyt *c* on different modified electrodes were studied by CV (shown in Fig. 5A). No distinct peaks appeared when there was no Cyt *c* on the bare GCE (a) or on PTCA-graphene/GCE (c). The response of Cyt *c*/GCE demonstrated a slender pair of peaks (b) which can hardly be observed compared to those of Cyt *c*/PTCA-graphene (e) and Cyt *c*/graphene (d). It suggested that the materials of PTCA-graphene and graphene can promoted the DET between Cyt *c* and electrode to some extent. It was noticeable that a well defined pair of quasi-reversible redox peaks could be observed on Cyt *c*/PTCA-graphene/GCE (e) which was attributed to the redox of the electro-active center of immobilized Cyt *c*. It indicated that DET had been achieved between Cyt *c* and the obtained electrodes [46]. The anodic peak potential (E_{pa}) and cathodic peak potential (E_{pc}) were located at 0.095 and 0.015 V, respectively. The 80 mV (ΔE_p) separation of anodic and cathodic peak potentials indicated a fast electron transfer reaction. And the ratio of cathodic to anodic current was about 1:1. The formal potential ($E^{\circ\prime}$) calculated by averaging the cathodic and anodic peak potentials was estimated as 55 mV. It is obviously that, as a contrast, the response of Cyt *c*/graphene/GCE (d) was lower than that of Cyt *c*/PTCA-graphene/GCE (e). It substantiated that PTCA-graphene composite which tended to form single layers was a preferable material for the DET between protein and electrodes as well as a advisable biocompatible substrate for Cyt *c* molecules. It might be owned to the excellent conductivity and high loading capacity of Cyt *c* molecules on these single-layer PTCA-graphene sheets. Boland et al. have proved concretely that the resistivity of individual graphene sheets scaled as their thickness increased from a single monolayer to larger thickness [47]. So the single-layer sheets attained very low interflake resistance values and the electrons transfer will be more efficiently within these sheets. On the other hand, since there was minute overlap or folding and more

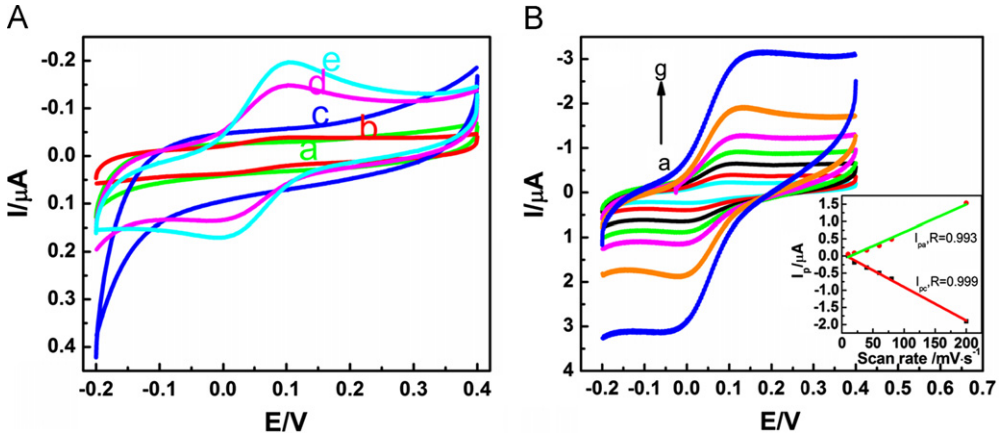

Fig. 5. (A) CVs of bare GCE (a, green), Cyt *c*/GCE (b, red), PTCA-graphene/GCE (c, blue), Cyt *c*-graphene/GCE (d, pink) and Cyt *c*/PTCA-graphene/GCE (e, cyan) with a scan rate of 10 mV/s, (B) CVs of Cyt *c* at various scan rates of 10, 20, 40, 60, 80, 100, 200 mV/s from (a) to (g) (inset: the relationship between the peak current I_p *vs.* the sweep rates V). (For interpretation of the references to color in this figure legend, the reader is referred to the web version of this article.)

negatively charged sites originated from PTCA, PTCA-graphene can provide a higher surface area for loading of Cyt *c* molecules.

CVs shown in Fig. 5B substantiated the dependence of redox peak currents and potentials of Cyt *c*/PTCA-graphene/GCE on the scan rates. With the increasing of the scan rates, the redox peak currents increased and the potentials shifted simultaneously while ΔE_p became greater. Both the cathodic and anodic peaks currents were linearly proportional to the scan rate ranging from 10 to 200 mV/s with correlation coefficients of 0.993 and 0.999, respectively (shown in the inset of Fig. 5B). It demonstrated a surface-controlled electrochemical process and a stable immobilization of Cyt *c* on the electrode surface.

3.5. Influence of pH on the DET of Cyt c

The effect of pH to the potential of Cyt *c* modified electrode was investigated in different buffer solutions in the absence of oxygen. CVs of Cyt *c* modified electrode showed great dependence on pH of external buffers (Fig. 6A) as reported [48–50]. Both reduction and oxidation peak potentials of the Fe^{III}/Fe^{II} redox couple of Cyt on PTCA-graphene modified GCE migrated negatively when pH increased. The linear correlation (Fig. 6B) between E and pH were expressed as follows: $E=-58.43\ pH+533.57$, $R^2=0.989$. This slope was close to the theoretical value -59 mV, which indicated a one-proton and one-electron process [51–53].

3.6. Electro-catalysis of Cyt c/PTCA-graphene/GCE to the reduction of H_2O_2

In order to investigate the electro-catalytic activity of the Cyt *c* on the modified electrode, its response to the reduction of H_2O_2 was studied by CV (Fig. 7).

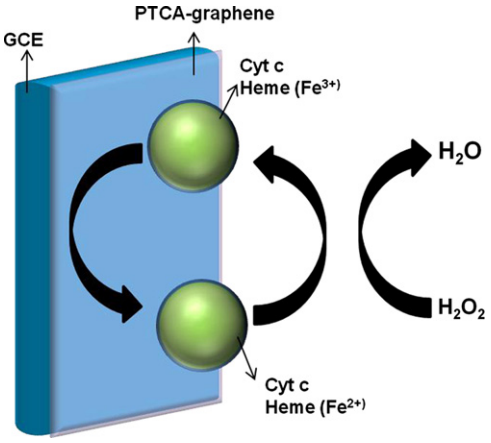

Scheme 2. Illustration of electro-catalytic principle of H_2O_2 on Cyt *c*/PTCA-graphene/GCE.

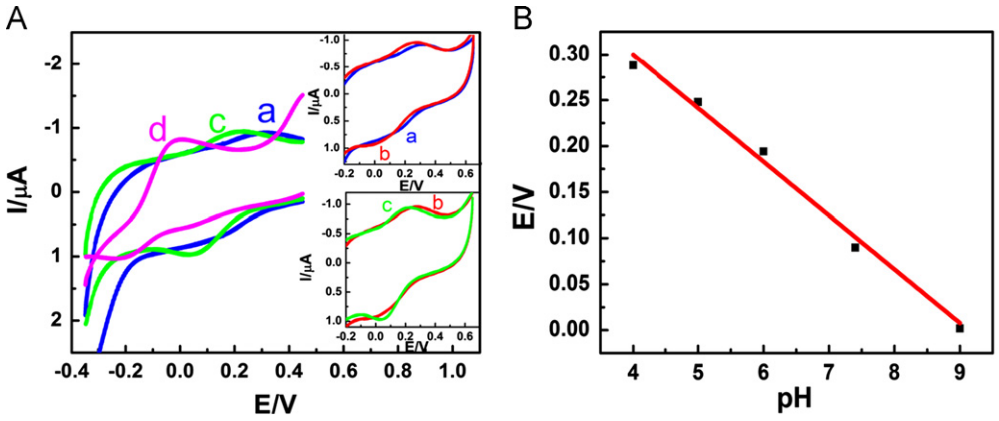

Fig. 6. (A) CVs of a Cyt *c*/PTCA-graphene/GCE in different buffer solution of pH 4 (a, blue), pH 5 (b, red), pH 6 (c, green), pH 9 (d, pink). (B) Effect of pH on the formal potential of the Cyt *c*/PTCA-graphene/GCE. (For interpretation of the references to color in this figure legend, the reader is referred to the web version of this article.)

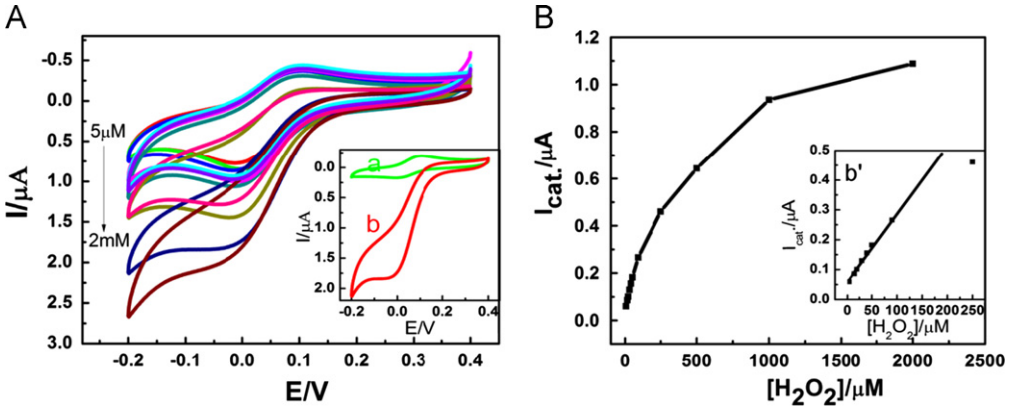

Fig. 7. (A) CVs of a Cyt *c*/PTCA-graphene/GCE at 10 mV/s in PBS containing H_2O_2 at the concentrations of 5, 15, 20, 30, 40, 50, 90, 250, 500, 1000, 2000 μM, respectively (inset: CVs of Cyt *c*/PTCA-graphene/GCE in the absence (a) and in presence of H_2O_2 with a concentration of 1000 μM (b) at a scan rate of 10 mV/s). (B) Calibration curve of concentrations *vs.* I_p (the inset: the linear curve of concentrations *vs.* I_p).

Table 1
Comparison of different Cyt *c* modified electrode for H_2O_2 determination.

Electrode	Line range (μM)	Detection limit (μM)	Sensitivity (μA/cm^2/mM)	Relative standard deviation	Reference
Cyt *c*/GNPs/RTIL/MWNT/GCE	50 to 1,150	3			[5]
Cyt *c*/Chit-Aus/Cys/Au	85 to 1,300	9.8			[49]
Cyt *c*/Au-NR	50 to 1,500	3.7	7	< 5%	[54]
Cyt *c*/CoO_x NPs/GCE	30 to 12,000	80	0.37	2.3%	[57]
Cyt *c*/MPCE	20 to 240	14.6	0.045		[58]
Cyt *c*/PTCA-graphene/GCE	5 to 90	3.5	0.0244	2.39%	Present work

RTIL: room temperature ionic liquid; Chit-Aus: chitosan-stabilized gold nanoparticles; Cys: cysteine; Au-NR: nanorod-like gold electrode; CoO_x NPs: cobalt oxide nanoparticles; MPCE: macroporous carbon electrode.

In the absence of H_2O_2, only the redox peaks of Cyt *c* were observed (shown as curve *a*, inset of Fig. 7A). While upon the addition of 1000 μM H_2O_2 to the buffer solution (curve *b*, inset of Fig. 7A), the voltammetric behavior of the modified electrode changed dramatically. CV curve with a great increasing of the catalytic reduction peak and an obvious decreasing of the oxidation peak can be observed. The causation of changes on the redox current can be explained by Scheme 2. The mechanism of this kind of reaction has been investigated by many researchers [17,54–56]. Typically, H_2O_2 can oxidize Cyt *c*-Heme (Fe^{2+}) and transferred it to Cyt *c*-Heme (Fe^{3+}) quickly (1) while Cyt *c*-Heme (Fe^{3+}) will be directly electrochemically reduced to Cyt *c*-Heme (Fe^{2+}) on the surface of the electrode (2). The presence of H_2O_2 increased the concentration of Cyt *c*-Heme (Fe^{3+}) and decreased that of Cyt *c*-Heme (Fe^{2+}) on the surface of the modified electrode and so caused the increasing of the reduction current and decreasing of the oxidation current. And formula (3) was the process of electro-catalytic reduction of H_2O_2 by Cyt *c*. The change of redox current validated the DET between active center and electrode as well as the electro-catalytic activity of Cyt *c* towards reduction of H_2O_2.

$$\text{Cyt } c\text{-Heme}(Fe^{2+}) + 1/2H_2O_2 + H^+ \rightarrow \text{Cyt } c\text{-Heme } (Fe^{3+}) + H_2O \quad (1)$$

$$\text{Cyt } c\text{-Heme}(Fe^{3+}) + e^- \rightarrow \text{Cyt } c\text{-Heme } (Fe^{2+}) \quad (2)$$

$$1/2H_2O_2 + H^+ + e^- \xrightarrow{\text{Cyt } c\text{-Heme } (Fe^{3+/2+})} H_2O \quad (3)$$

Fig. 7A shows the CVs of the Cyt *c*/PTCA-graphene/GCE when the concentration of H_2O_2 in PBS (0.1 M, pH 7.4) varied from 5 μm to 2 mM. The reduction current enhanced obviously while the oxidation peak current decreased with the increasing of H_2O_2. The curve of catalytic currents *vs.* H_2O_2 concentrations is shown in the inset of Fig. 7B and the linear range was found to be 5 to 90 μM (inset of Fig. 7B). The sensitivity was 0.0244 μA/cm^2/mM and the relative standard deviation was 2.39%. At the signal to noise ratio of 3, the detection limit was 3.5 μM.

High selectivity of the modified electrode was also confirmed. The experimental results showed that K^+, Na^+, Ca^{2+}, Cl^-, SO_4^{2-}, CO_3^{2-} at 10-fold concentration as high as that of H_2O_2 did not interfere in the determination of H_2O_2. No interference could be observed for ascorbic acid (AA), glucose and dopamine as well.

Comparing with other kinds of Cyt *c* modified electrodes, Cyt *c*/PTCA-graphene/GCE could provide higher sensitivity, comparable detection limit and excellent signal response in the relative low concentration range (Table 1).

4. Conclusion

In summary, graphene has been successfully functionalized by PTCA and the resulting PTCA-graphene composite was proved to be stably and uniformly dispersed in aqueous solution. This kind of material can provide high surface area and preferable biocompatibility for immobilization of Cyt *c*. PTCA with plenty of –COOH groups provided more active sites for the loading of protein molecules due to the electrostatic adsorption between Cyt *c* and PTCA-graphene. Above all, it has been proved that the as prepared PTCA-graphene acted as both an excellent biocompatible substrate for Cyt *c* molecules and "conducting wire" which exhibited a high electrochemical activity for promoting the DET of Cyt *c*. The heme containing Cyt *c* in the composite maintained its natural active characteristic, exhibiting the electrochemical catalytic activity to the reduction of H_2O_2. Based on these points, PTCA-graphene can be a preferable material for the potential application of Cyt *c* based biosensors.

Acknowledgement

The authors are most grateful to the NSFC (No.21175130, No.21105096 and No.21205112) and Department of Science and Technology of Jilin Province (No.201215091 and No.20120308) and Department of Science and Technology of Changzhou City (CJ20110016) for their financial support.

References

[1] Y. Zhou, J. Zhi, Y. Zou, W. Zhang, S.-T. Lee, Anal. Chem. 80 (2008) 4141–4146.
[2] Q. Chen, S. Ai, X. Zhu, H. Yin, Q. Ma, Y. Qiu, Biosens. Bioelectron. 24 (2009) 2991–2996.
[3] W.C. Alvin Koh, M.A. Rahman, E.S. Choe, D.K. Lee, Y.-B. Shim, Biosens. Bioelectron. 23 (2008) 1374–1381.
[4] M.K. Beissenhirtz, F.W. Scheller, F. Lisdat, Anal. Chem. 76 (2004) 4665–4671.
[5] C. Xiang, Y. Zou, L.-X. Sun, F. Xu, Electrochem. Commun. 10 (2008) 38–41.
[6] R. Andreu, E.E. Ferapontova, L. Gorton, J.J. Calvente, J. Phys. Chem. B 111 (2006) 469–477.
[7] L. Wang, Electrochem. Commun. 6 (2004) 225–229.
[8] Y. Li, J. Li, X.-H. Xia, S.-Q. Liu, Talanta 82 (2010) 1164–1169.
[9] A. Mohammadi, A.B. Moghaddam, S. Ahadi, R. Dinarvand, A.A. Khodadadi, J. Appl. Electrochem. 41 (2010) 115–121.
[10] C. Mu, Q. Zhao, D. Xu, Q. Zhuang, Y. Shao, J. Phys. Chem. B 111 (2007) 1491–1495.
[11] J. Wang, M. Li, Z. Shi, N. Li, Z. Gu, Anal. Chem. 74 (2002) 1993–1997.
[12] S. Boussaad, N.J. Tao, R. Zhang, T. Hopson, L.A. Nagahara, Chem. Commun. (2003) 1502–1503.
[13] G.-C. Zhao, Z.-Z. Yin, L. Zhang, X.-W. Wei, Electrochem. Commun. 7 (2005) 256–260.
[14] W.J. Albery, M.J. Eddowes, H.A.O. Hill, A.R. Hillman, J. Am. Chem. Soc. 103 (1981) 3904–3910.
[15] S. Song, R.A. Clark, E.F. Bowden, M.J. Tarlov, J. Phys. Chem. 97 (1993) 6564–6572.
[16] A. El Kasmi, J.M. Wallace, E.F. Bowden, S.M. Binet, R.J. Linderman, J. Am. Chem. Soc. 120 (1998) 225–226.
[17] S. Ignatov, D. Shishniashvili, B. Ge, F.W. Scheller, F. Lisdat, Biosens. Bioelectron. 17 (2002) 191–199.
[18] M. Cortina-Puig, X. Muñoz-Berbel, R. Rouillon, C. Calas-Blanchard, J.-L. Marty, Bioelectrochemistry 76 (2009) 76–80.
[19] F.A. Armstrong, H.A.O. Hill, B.N. Oliver, J. Chem. Soc., Chem. Commun. (1984) 976–977.
[20] M. Fedurco, Coord. Chem. Rev. 209 (2000) 263–331.
[21] G. Wang, J.-J. Xu, H.-Y. Chen, Electrochem. Commun. 4 (2002) 506–509.
[22] S. Haymond, G.T. Babcock, G.M. Swain, J. Am. Chem. Soc. 124 (2002) 10634–10635.

[23] S. Alwarappan, R.K. Joshi, M.K. Ram, A. Kumar, Appl. Phys. Lett. 96 (2010) 263702.
[24] S. Stankovich, D.A. Dikin, G.H.B. Dommett, K.M. Kohlhaas, E.J. Zimney, E.A. Stach, R.D. Piner, S.T. Nguyen, R.S. Ruoff, Nature 442 (2006) 282–286.
[25] H. Chen, M.B. Müller, K.J. Gilmore, G.G. Wallace, D. Li, Adv. Mater. 20 (2008) 3557–3561.
[26] C. Shan, H. Yang, D. Han, Q. Zhang, A. Ivaska, L. Niu, Biosens. Bioelectron. 25 (2010) 1070–1074.
[27] C. Shan, H. Yang, J. Song, D. Han, A. Ivaska, L. Niu, Anal. Chem. 81 (2009) 2378–2382.
[28] H. Xu, H. Dai, G. Chen, Talanta 81 (2010) 334–338.
[29] Q. Lu, X. Dong, L.-J. Li, X. Hu, Talanta 82 (2010) 1344–1348.
[30] L. Tang, Y. Wang, Y. Li, H. Feng, J. Lu, J. Li, Adv. Funct. Mater. 19 (2009) 2782–2789.
[31] R.S. Dey, C.R. Raj, J. Phys. Chem. C 114 (2010) 21427–21433.
[32] S. Niyogi, E. Bekyarova, M.E. Itkis, J.L. McWilliams, M.A. Hamon, R.C. Haddon, J. Am. Chem. Soc. 128 (2006) 7720–7721.
[33] Y. Si, E.T. Samulski, Nano Lett. 8 (2008) 1679–1682.
[34] S. Stankovich, R.D. Piner, X.Q. Chen, N.Q. Wu, S.T. Nguyen, R.S. Ruoff, J. Mater. Chem. 16 (2006) 155–158.
[35] Y. Xu, H. Bai, G. Lu, C. Li, G. Shi, J. Am. Chem. Soc. 130 (2008) 5856–5857.
[36] F. Li, H. Yang, C. Shan, Q. Zhang, D. Han, A. Ivaska, L. Niu, J. Mater. Chem. 19 (2009) 4022–4025.
[37] Y. Hu, F. Li, X. Bai, D. Li, S. Hua, K. Wang, L. Niu, Chem. Commun. 47 (2011) 1743–1745.
[38] N.I. Kovtyukhova, P.J. Ollivier, B.R. Martin, T.E. Mallouk, S.A. Chizhik, E.V. Buzaneva, A.D. Gorchinskiy, Chem. Mater. 11 (1999) 771–778.
[39] X. Wang, S.M. Tabakman, H. Dai, J. Am. Chem. Soc. 130 (2008) 8152–8153.
[40] M. Hara, A. Satoh, N. Takami, T. Ohsaki, J. Phys. Chem. 99 (1995) 16338–16343.
[41] S. Stankovich, D.A. Dikin, R.D. Piner, K.A. Kohlhaas, A. Kleinhammes, Y. Jia, Y. Wu, S.T. Nguyen, R.S. Ruoff, Carbon 45 (2007) 1558–1565.
[42] D. Li, M.B. Müller, S. Gilje, R.B. Kaner, G.G. Wallace, Nat. Nanotechnol. 3 (2008) 101–105.
[43] M. Collinson, E.F. Bowden, Anal. Chem. 64 (1992) 1470–1476.
[44] G. Irace, E. Bismuto, F. Savy, G. Colonna, Arch. Biochem. Biophys. 244 (1986) 459–469.
[45] J. Zhou, X. Lu, J. Hu, J. Li, Chem. Eur. J 13 (2007) 2847–2853.
[46] C. Xiang, Y. Zou, L.X. Sun, F. Xu, Talanta 74 (2007) 206–211.
[47] P.N. Nirmalraj, T. Lutz, S. Kumar, G.S. Duesberg, J.J. Boland, Nano Lett. 11 (2010) 16–22.
[48] A.E.F. Nassar, Z. Zhang, N.F. Hu, J.F. Rusling, T.F. Kumosinski, J. Phys. Chem. B 101 (1997) 2224–2231.
[49] J.J. Feng, G. Zhao, J.J. Xu, H.Y. Chen, Anal. Biochem. 342 (2005) 280–286.
[50] F. Paulo, I.C.N. Diogenes, H.D. Abruna, Langmuir: ACS J. Surf. Colloids 27 (2011) 2052–2057.
[51] L. Meites, Polarographeic Techniques, second ed., Wiley, New York, 1965 282-284.
[52] A.M. Bond, Modern Polarographeic Methods in Analytical Chemistry, Marcel Dekker, New York, 1980, pp. 29–30.
[53] A. Salimi, E. Sharifi, A. Noorbakhsh, S. Soltanian, Biophys. Chem. 125 (2007) 540–548.
[54] H. Liu, Y. Tian, Z. Deng, Langmuir 23 (2007) 9487–9494.
[55] A.B. Moghaddam, M.R. Ganjali, R. Dinarvand, S. Ahadi, A.A. Saboury, Biophys. Chem. 134 (2008) 25–33.
[56] M. Cortina-Puig, X. Munoz-Berbel, R. Rouillon, C. Calas-Blanchard, J.-L. Marty, Bioelectrochemistry 76 (2009) 76–80.
[57] A. Mohammadi, A.B. Moghaddam, S. Ahadi, R. Dinarvand, A.A. Khodadadi, J. Appl. Electrochem. 41 (2011) 115–121.
[58] L. Zhang, Biosens. Bioelectron. 23 (2008) 1610–1615.